Electronic Supplementary Material (ESI) for Journal of Materials Chemistry A.
This journal is © The Royal Society of Chemistry 2023

Supporting Information

Flexible nanocellulose-based layered films by crosslinking phosphorous lignin nanoparticles and functionalized boron nitride nanosheets for flame-resistant, and thermally conductive application

Bingyang Liu[a,b], Jinsong Zeng[a,b,*], Pengfei Li[a,b,c,*], Jinpeng Li[a,b], Bin Wang[a,b], Jun Xu[a,b], Wenhua Gao[a,b], and Kefu Chen[a,b]

[a] Plant Fiber Material Science Research Center, State Key Laboratory of Pulp and Paper Engineering, School of Light Industry and Engineering, South China University of Technology, Guangzhou 510640, P.R. China.

[b] Guangdong Provincial Key Laboratory of Plant Resources Biorefinery, Guangzhou 510640, P.R. China.

[c] School of Environment and Energy, South China University of Technology, Guangzhou 510640, P.R. China.

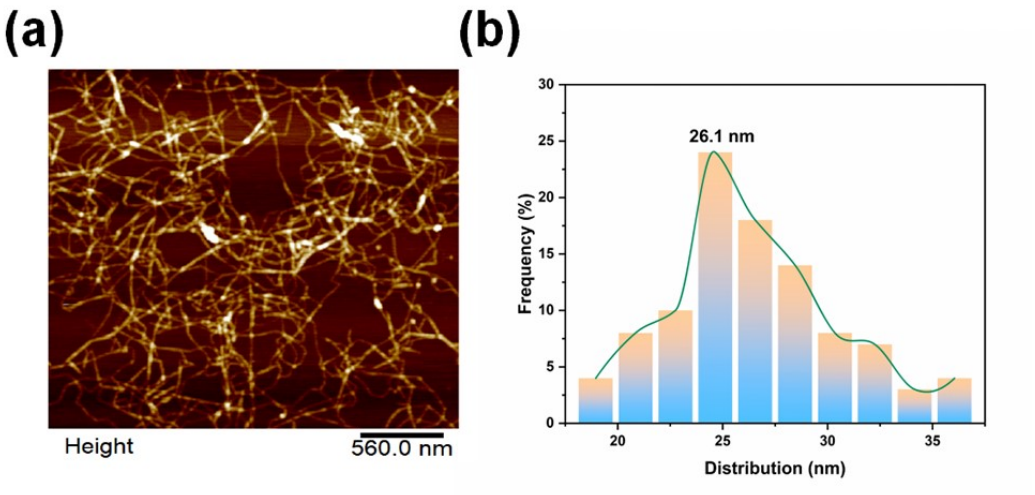

Fig. S1. AFM image (a) and average diameter (b) of TOCNF.

The nanocellulose has been prepared by TEMPO-mediated oxidation using the TEMPO/NaBr/NaClO system. The pine wood pulp was dispersed in deionized water at a concentration of 1.0wt%, and then the TEMPO (16 mg g^{-1} cellulose) and NaBr (100 mg g^{-1} cellulose) were added to the dispersion. During continuous stirring, NaClO (7.5 mmol g^{-1} cellulose) was slowly added into the dispersion. The oxidized reaction was carried out at pH 10.0 for 3 h, which was adjusted using NaOH solution (0.5 mol L^{-1}). After the reaction, the product was repeatedly washed with deionized water to neutralize, and finally, the TEMPO oxidation nanocellulose fibers (TOCNF) were obtained by mechanical treatment with a high-speed shear machine. TOCNF was dispersed in deionized water at a concentration of 0.5wt% for further use. The content of sodium carboxylate groups and crystallinity index in the TOCNF was 0.85 mmol/g and 63.6%, respectively. The microstructure and diameter distribution of the TOCNF are shown in **Fig. S1**. TOCNF had a uniform diameter of 26.1 ± 5.0 nm and several

hundred nanometers in length.

Preparation of Phosphated Lignin Nanoparticles

First, in a 250ml flask, the organic soft lignin powder (OSL 1.0g) was added to A mixture of 100ml acetone and water (A/W=7:3). The lignin was dissolved by magnetic stirring for 1 hour at ambient temperature. LNPs were prepared based on the solvent-antisolvent method, LNPs were prepared from 10 mL of 10.00 g/L lignin solution in 7:3 (v/v) A/W by nanoprecipitation. The solution was slowly added to 200 mL DI water for 1 min under mechanical agitation at 500 rpm (**Fig. S2**). Then, H_3PO_4 (mass ratio to lignin: 10/1) was dropped into the above solution and the mixed reaction solution was maintained at 60 ℃ for a whole night. Finally, the mixed solution was filtered, washed, and freeze-dried to obtain phosphorous lignin nanoparticles (PL)

Fig. S2. The fabrication process of Phosphated Lignin Nanoparticles.

Characterization of Phosphated Lignin Nanoparticles

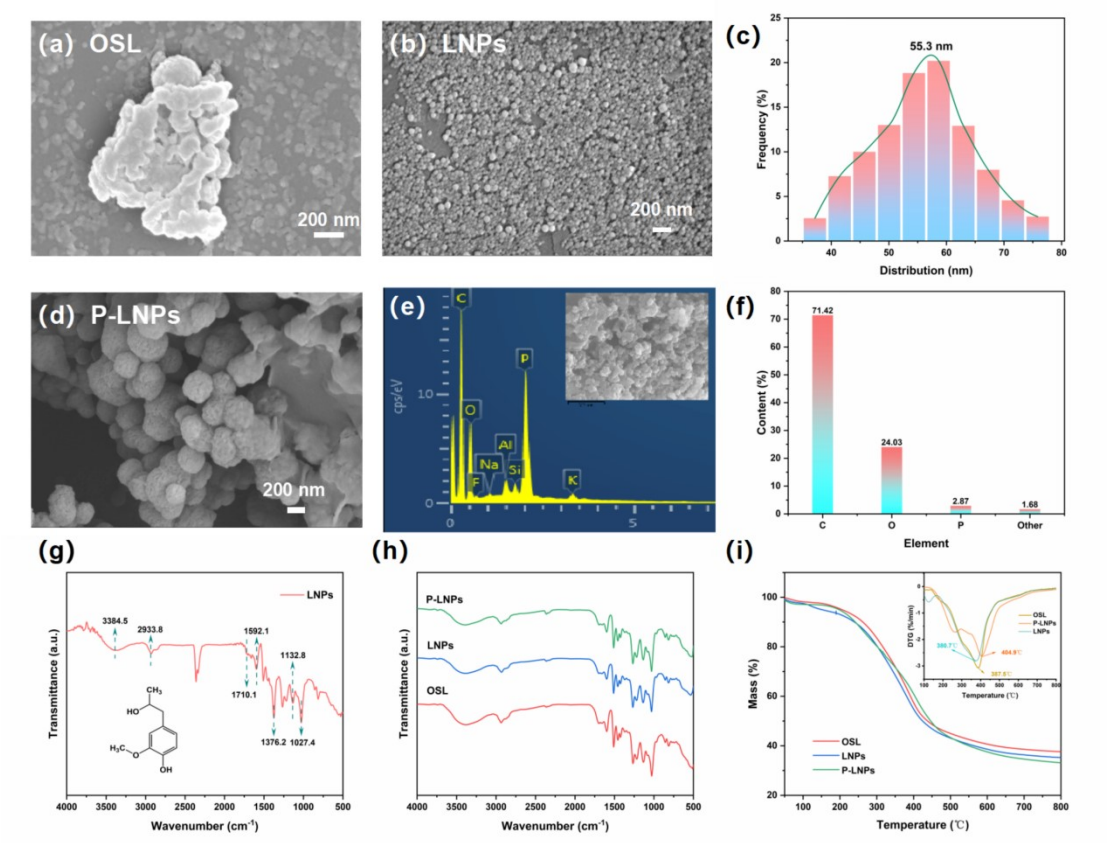

Fig. S3. SEM images of (a) OSL, (b) LNPs, and (d) P-LNPs. (c) The average diameter of LNPs. (e,f) EDS elemental mapping of P-LNPs. (g) FT-IR spectrum of LNPs; (h) FT-IR spectrum, (i) TG and DTG curves of OSL, LNPs, and P-LNPs.

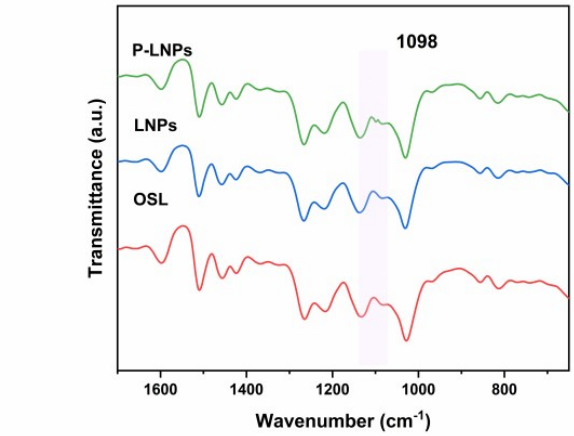

Fig. S4. FT-IR spectrum of OSL, LNPs, and P-LNPs.

SEM method was used to characterize the morphology of OSL, LNPs, and PL, the morphology is shown in **Fig. S3a-d**. The original lignin showed large irregular morphology, and the lignin was transformed into nanoparticles with uniform size distribution after anti-solvent treatment. The surface of lignin nanoparticles becomes rough after phosphating treatment, which may be due to the deposition of phosphorus-containing groups, and EDS results can also prove this conclusion (**Fig. S3e-f**). By comparing the infrared spectra of the obtained samples, it was found that the lignin structure had a typical lignin structure, and there was no significant change after the treatment, which may be attributed to the fact that the original lignin did not form obviously new structure after the nano and phosphatization treatment. With the introduction of H_3PO_4, the FT-IR spectra of the lignin samples did not change significantly; only the characteristic peak of phospholipid groups was observed at 1098 cm^{-1} (**Fig. S4**). Finally, by comparing the thermal stability of the obtained samples, it can be found that PL has a higher thermal decomposition temperature, which is conducive to improving the flame retardancy of composite films containing PL.

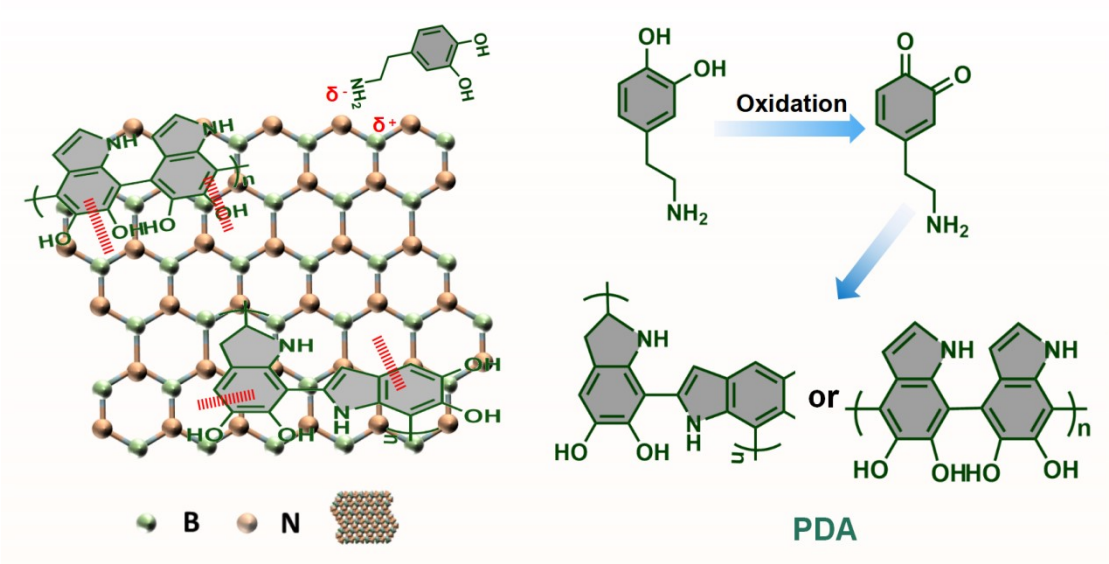

Scheme S1 Schematic illustration of intermolecular forces between BN and PDA and the surface modification of BN and the mechanism of polymerization.

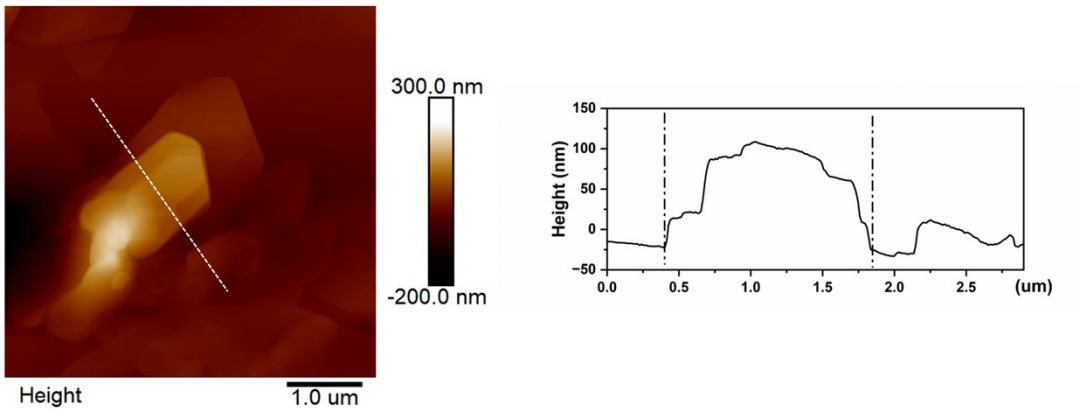

Fig. S5. AFM image of h-BN.

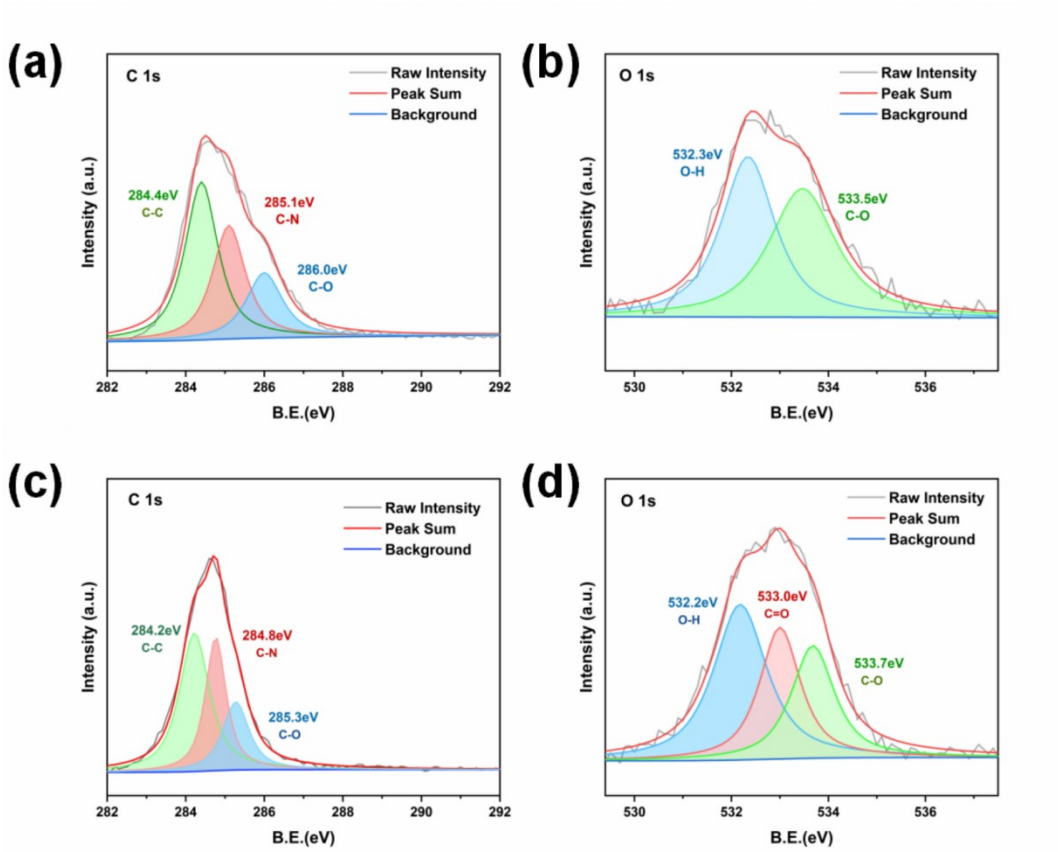

Fig. S6. XPS spectra of C1s (a) h-BN, (c) BNNS@PDA, and O1s (b) h-BN, (d) BNNS@PDA.

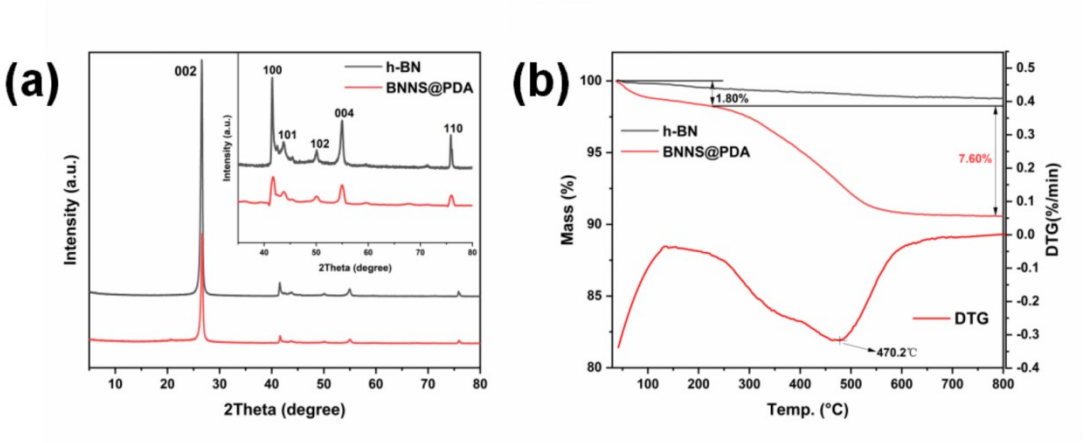

Fig. S7. (a) XRD patterns, (b) TGA curves at nitrogen atmosphere of h-BN and BNNS@PDA.

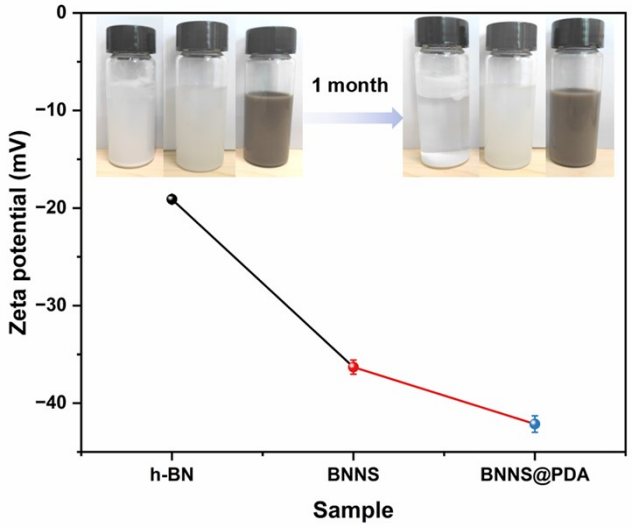

Fig. S8. Zeta potential of h-BN, BNNS, and BNNS@PDA.

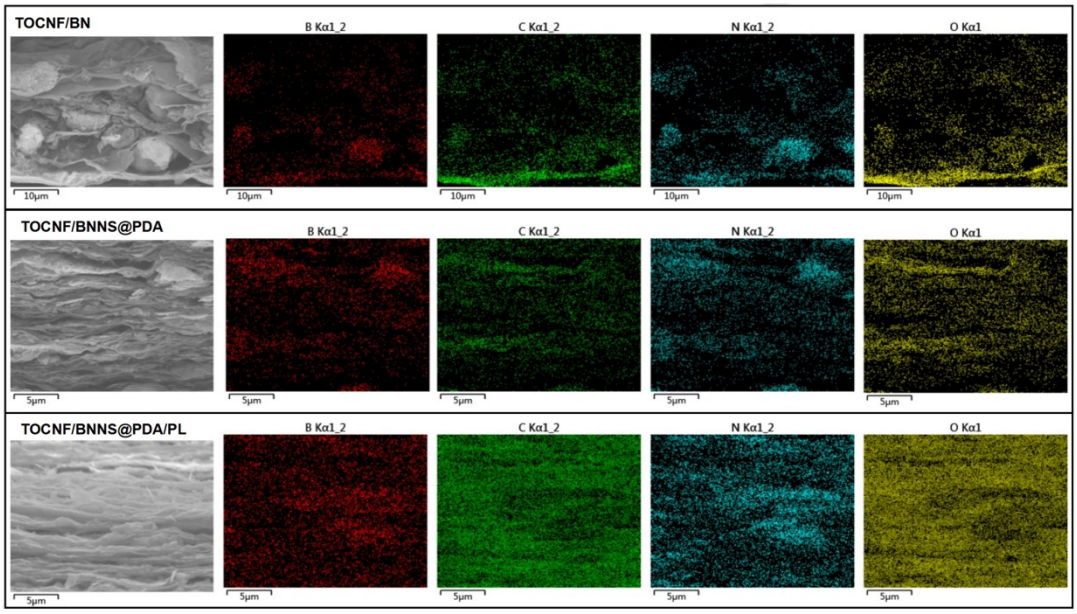

Fig. S9. Cross-sectional SEM image and EDS of TOCNF-based composite films.

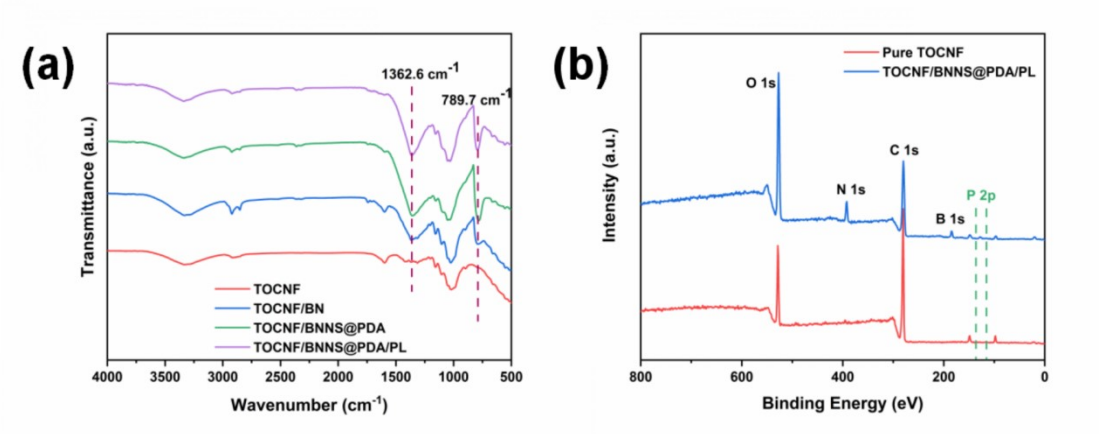

Fig. S10. Chemical structure of pure TOCNF and TOCNF-based composite films, (a) FTIR, (b) XPS spectra.

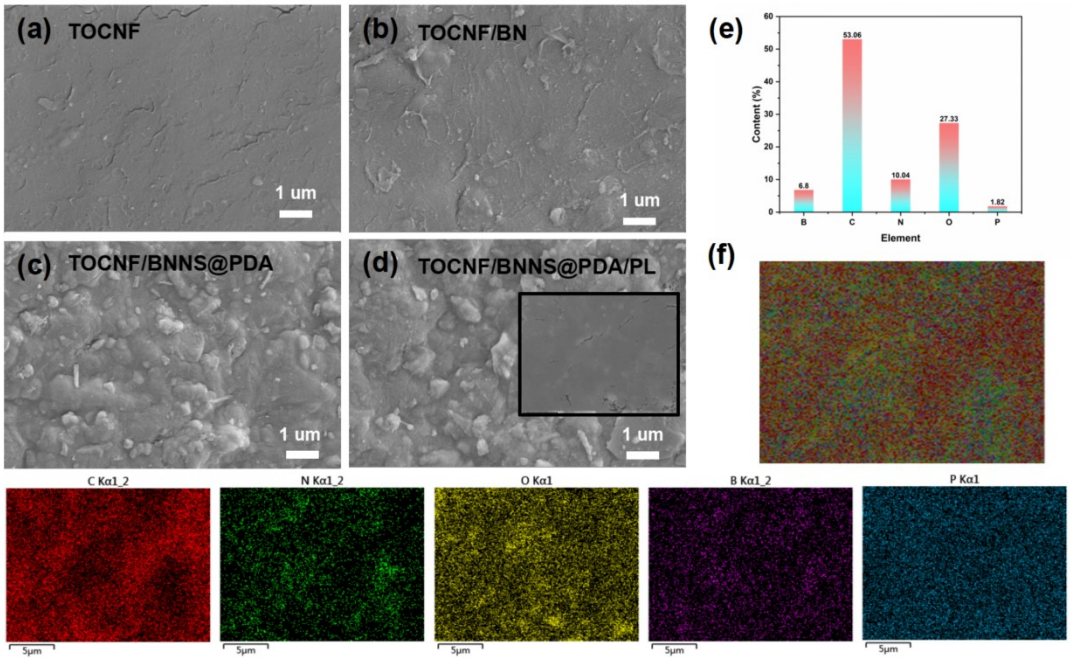

Fig. S11. (a-d) SEM images of pure TOCNF and TOCNF-based composite films, (e) Content of each element, and (f) EDS elemental mapping of TOCNF/BNNS@PDA/PL composite film.

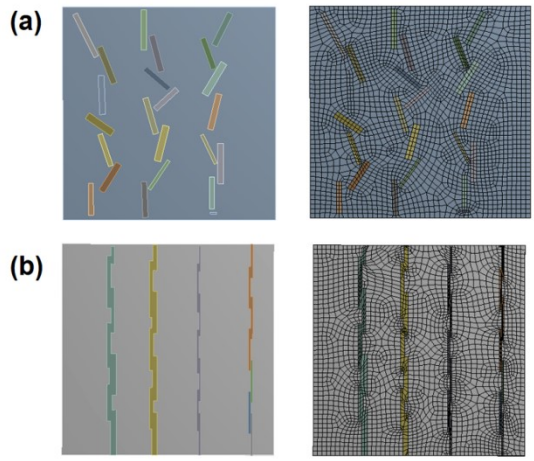

Fig. S12. The models and corresponding grid divisions of the (a) high- and (b) low-in-plane orientation BNNS@PDA are used in the ANSYS simulation.

The finite element simulation software (ANSYS) was employed to investigate the effect of aspect ratio on the heat transfer capabilities of the composites. In the typical process of simulation, a linear heat source (100 ℃) was set at the bottom of the model, and the convection coefficient of the exposed surface of the system was set to 10 W m^{-2} K^{-1} with a fixed ambient temperature of 25 ℃. The thermal conductivity of the BNNS and PVA matrix are set to 600 W m^{-1} K^{-1} and 0.3 W m^{-1} K^{-1}, respectively.

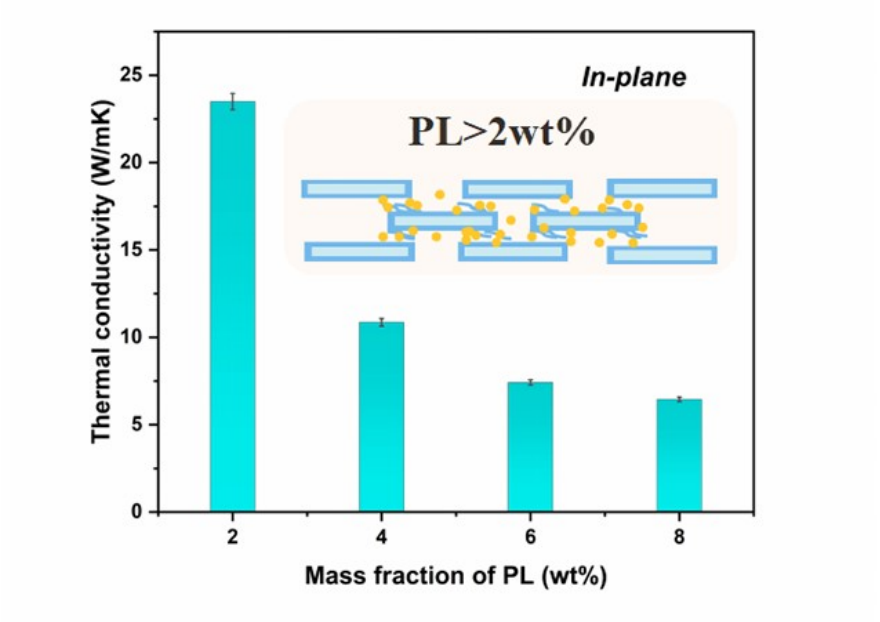

Fig. S13. In-plane thermal conductivity (TC) as a function of contents of PL.

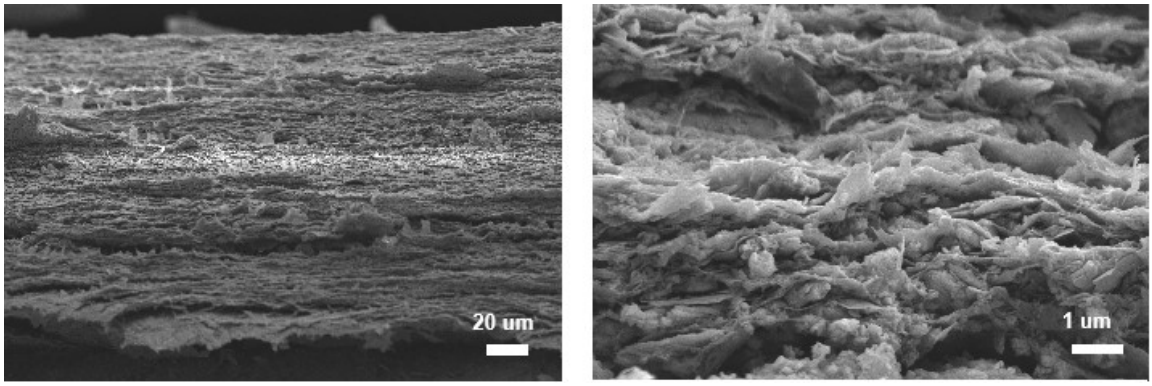

Fig. S14. Cross-sectional SEM image of TOCNF/BNNS@PDA composite films (70 wt% BNNS@PDA).

Theoretical analysis of the effect of the addition of PL on the heat transfer capability of the composites based on Foygel's nonlinear model.

When phonons propagate through interconnected BN networks in the composites, the contact resistance between partially overlapped BN dominates heat transfer efficiency of the composites. Such behavior of phonon transport between adjoining BNNS can be theoretically explained by Foygel's theory, which is defined as the following equations[1]:

$$k = k_0(V_f - V_c)^{\tau} \quad (1)$$

where k is the thermal conductivity of the composite films; k_0 is a pre-exponential factor ratio contributed by interconnected BN network; V_f is the measured volume fraction of BN in the composites; τ is the conductivity exponent determined by the aspect ratio of BN; $V_c$is the critical volume fraction of BN, which is the intercept of the tangent with the X-axis in the figure of thermal conductivity of the composites as a function of filler content. In our case, V_c for the case of TOCNF/BNNS@PDA and TOCNF/BNNS@PDA/2%PL is 1.039 vol% and 1.171 vol%, respectively

In order to obtain the values of k_0 and τ, the equation (1) needs to be transformed into a linear form:

$$lgk = lgk_0 + \tau lg(V_f - V_c) \quad (2)$$

where lgk is a linear function with the independent variable of BN content (V_f) in the composites, and, both lgk_0 and τ are the constant terms, which are equal to a and b in the linear equation of y = ax + b respectively. Accordingly, the values of k_0 and τ can be calculated by linear fitting the plots obtained from our experiments, as shown in **Fig. S15**

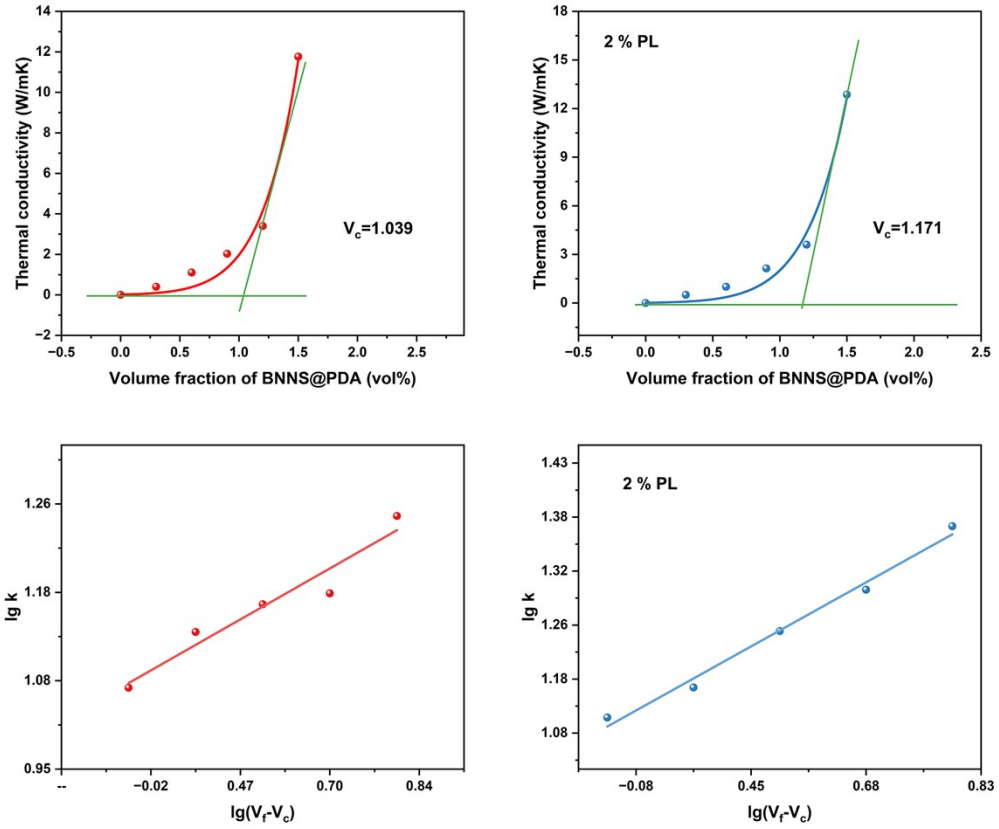

Fig. S15. The fitting results of experimental thermal conductivities of TOCNF/BNNS@PDA and TOCNF/BNNS@PDA/2%PL composites based on Foygel's physical model.

Based on the calculated values of k_0 and τ, we can obtain the contact resistance (R_c) between the adjacent BNNS@PDA by the following equation:

$$R_C = \frac{1}{k_0 L V_c^{\tau}} \tag{3}$$

L is the lateral size of BNNS@PDA, which of the TOCNF/BNNS@PDA and TOCNF/BNNS@PDA/2%PL are 0.31 and 0.31 μm (**Fig. S16**), respectively. As a result, the calculated R_C of TOCNF/BNNS@PDA is 2.9 × 10^5 KW^{-1}, which is higher than that of TOCNF/BNNS@PDA/2%PL (2.5 × 10^5 KW^{-1}).

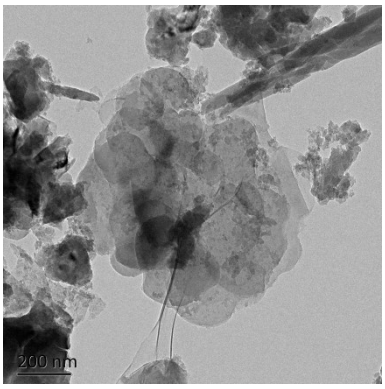

Fig. S16. The TEM image of BNNS@PDA nanosheets.

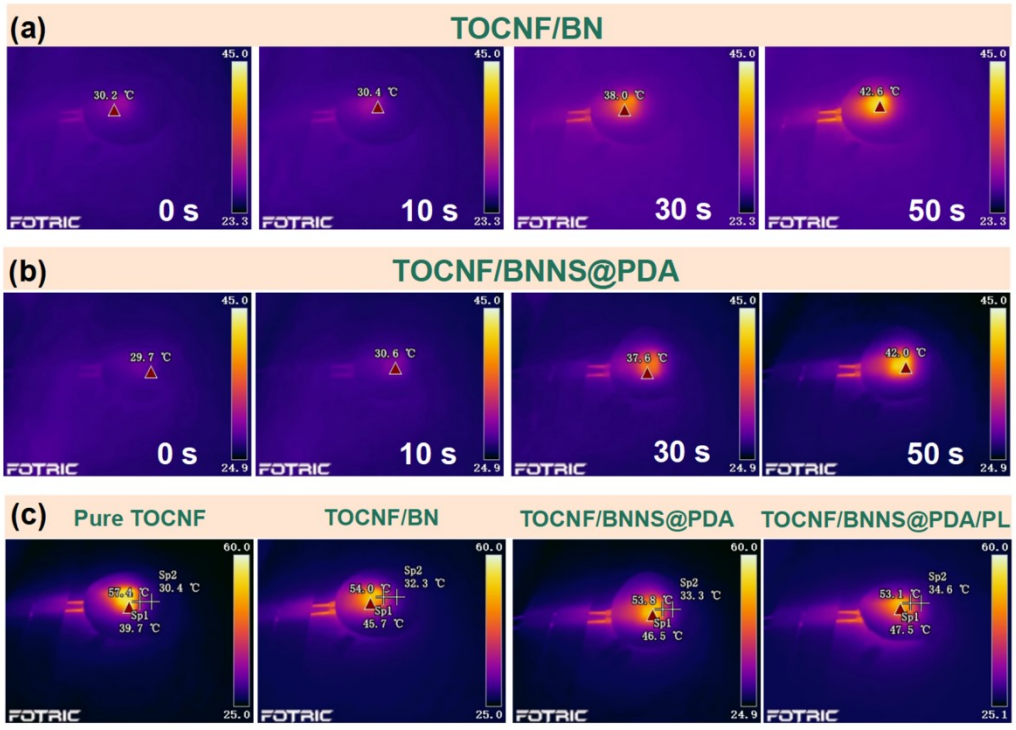

Fig. S17. (a-b) The infrared thermal images and central temperature variation of various composites. (c) The temperature of the edge (Sp1 and Sp2) and the center point of the pure TOCNF film and TOCNF/BNNS@PDA/PL composite films.

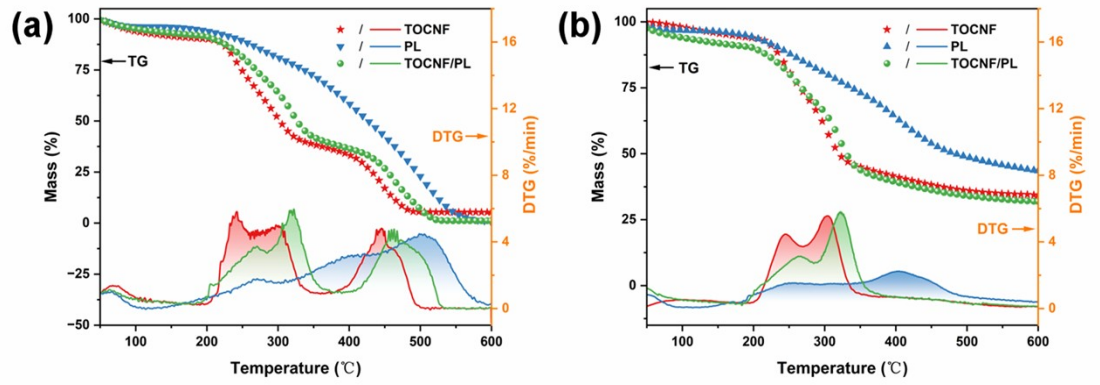

Fig. S18. TGA and DTG curves of pure TOCNF, PL and TOCNF/PL composite films (a) in air, (b) in N_2.

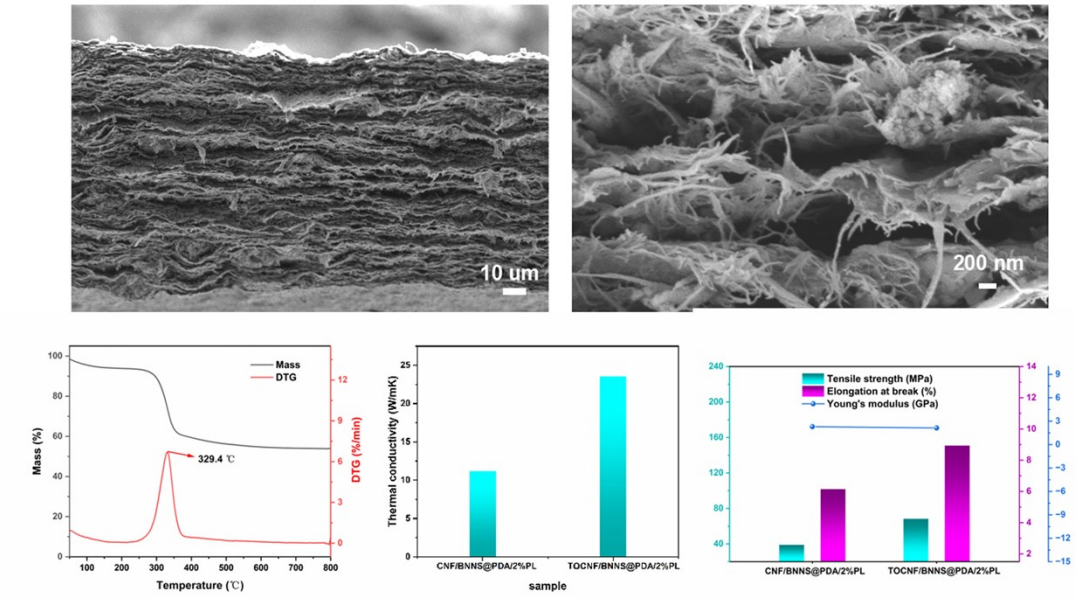

Fig. S19. Morphology and properties of the CNF/BNNS@PDA/2%PL composite films.

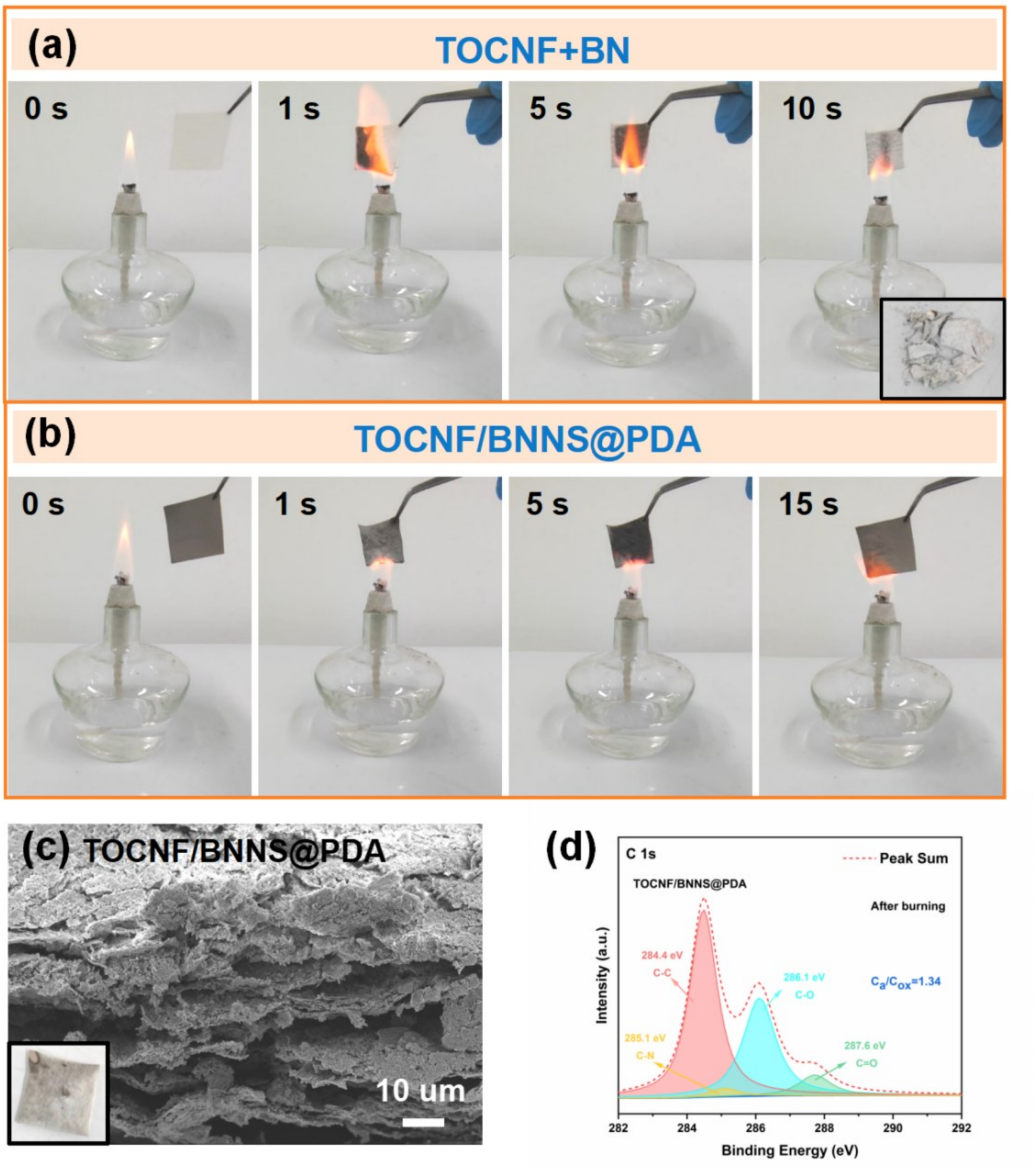

Fig. S20. Flame burning tests of (a) TOCNF/BN, (b) TOCNF/BNNS@PDA composite film. (c) Cross section of TOCNF/BNNS@PDA composite film after burning. (d) C1s XPS spectra of TOCNF/BNNS@PDA composite film after burning.

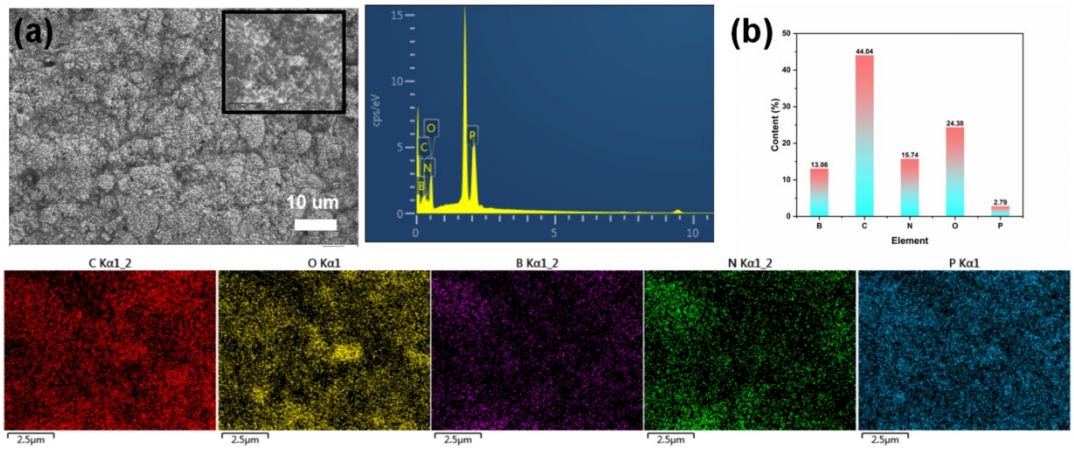

Fig. S21. (a) SEM images of the TOCNF/BNNS@PDA/PL composite film after flame treatment, showing relatively stable morphologies; (b) EDS elemental mapping of TOCNF/BNNS@PDA/PL composite film after flame treatment.

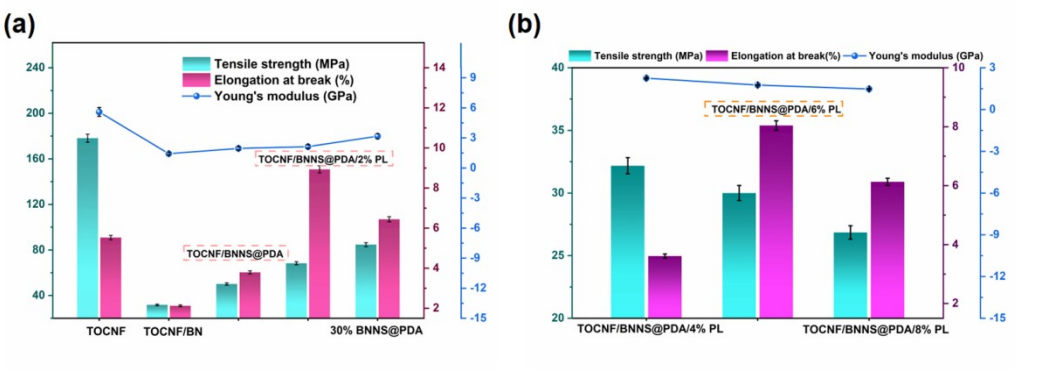

Fig. S22. (a) Corresponding mechanical parameters of the pure TOCNF and TOCNF-based composite films. (b) Stress-strain curves corresponding mechanical parameters of TOCNF/BNNS@PDA/PL composite films with different content of PL fillers including tensile strength, elongation at break, and work of fracture.

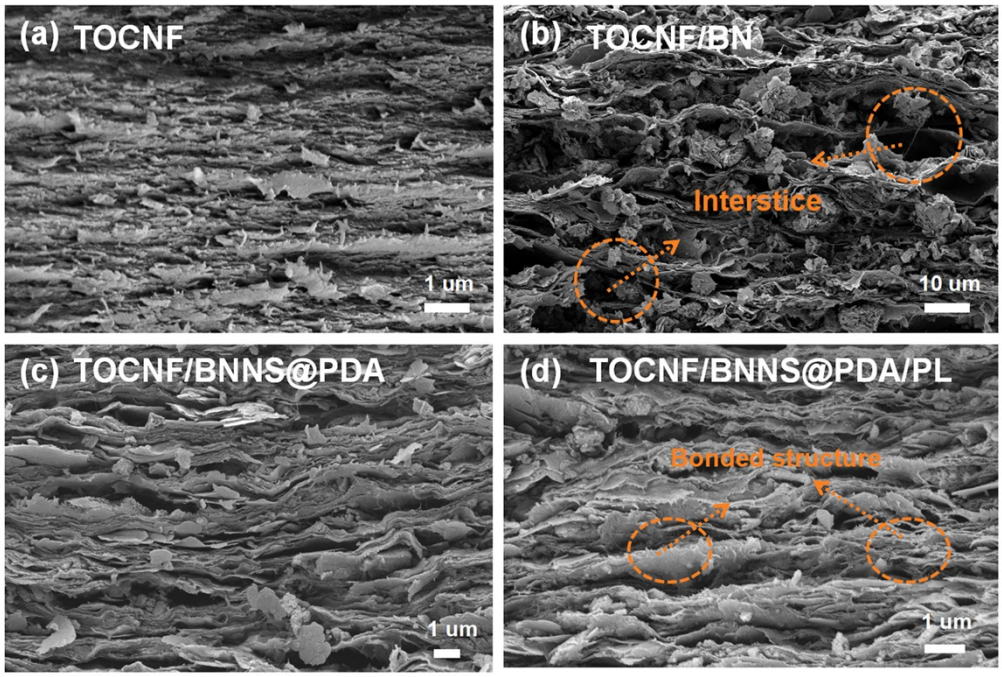

Fig. S23. Cross-sectional SEM images of the fracture surface of pure TOCNF film and TOCNF-based composite films.

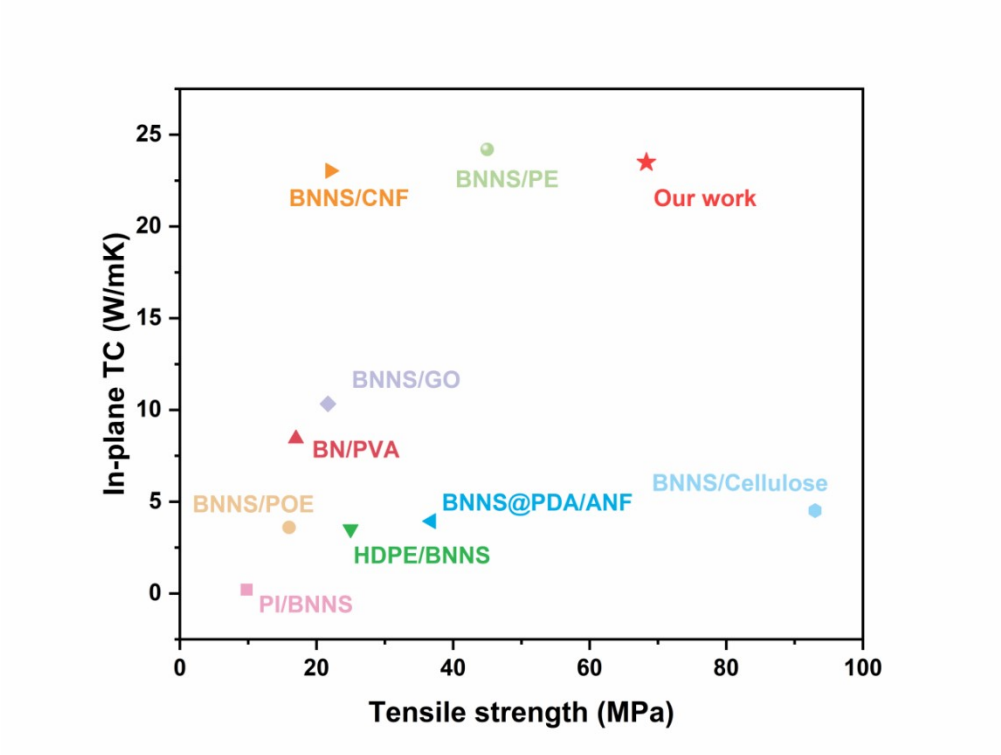

Fig. S24. Comparison of the in-plane thermal conductivity with polymer/BNNS

composites based on the reported studies.

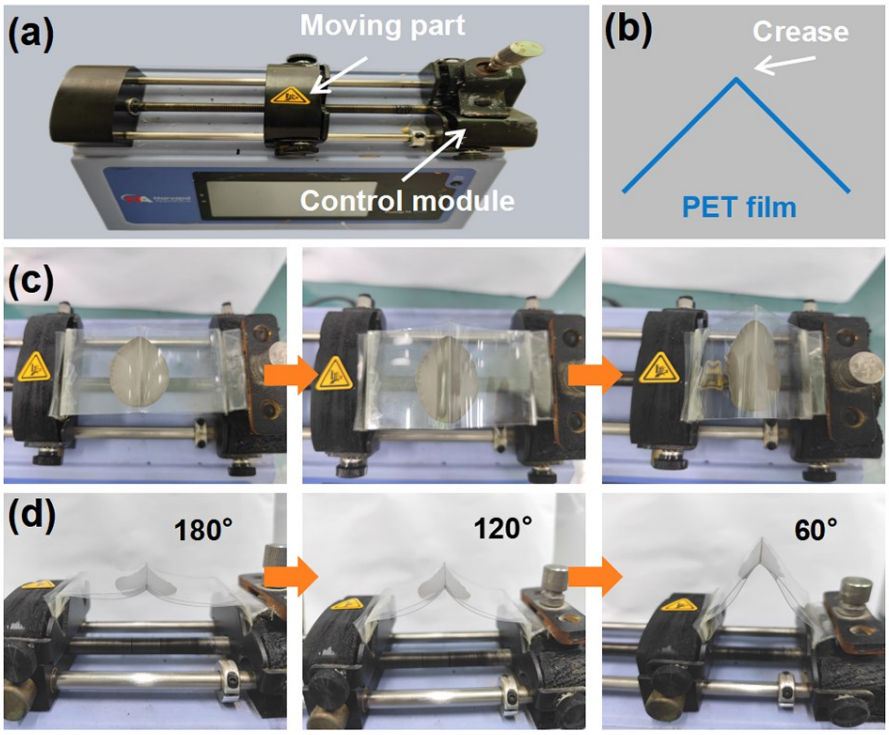

Fig. S25. Stress-strain curves corresponding mechanical parameters of TOCNF/BNNS@PDA/PL composite films with different content of PL fillers including tensile strength, elongation at break, and work of fracture.

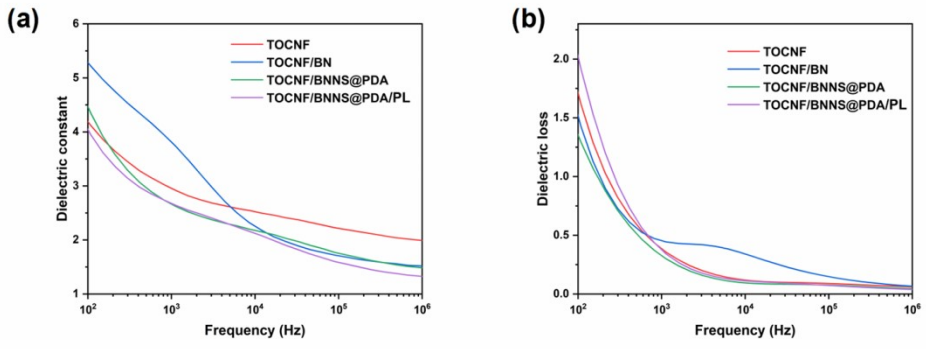

Fig. S26. (a) Dielectric constant, (b) Dielectric loss of the composite films.

Table S1. Chemical compositions of h-BN and BNNS@PDA based on the result of XPS spectra.

Sample	Atomic percent (%)			
	C	O	N	B
h-BN	4.91	52.6	22.45	20.05
BNNS@PDA	10.29	70.33	9.00	10.37

Table S2. The parameters for the calculation of in-plane thermal conductivities of pure TOCNF and different TOCNF-based composite films.

Sample	Thermal Diffusivity (mm^2s^{-1})	Specific heat capacity ($J\ g^{-1}\ K^{-1}$)	Density ($g\ cm^{-3}$)	Thermal conductivity ($W\ m^{-1}\ K^{-1}$)	BNNS@PDA content (wt%)	PL content (wt%)
TOCNF	0.78(0.01)	1.82	0.96	1.36(0.02)	0	0
TOCNF/BNa	1.92(0.09)	1.32	1.20	3.05(0.15)	0	0
TOCNF/BNNS@PDA	10.54(1.10)	1.36	1.23	17.59(1.84)	50	0
TOCNF/BNNS@PDA/2%PL	12.10(1.41)	1.29	1.50	23.49(2.73)	50	2
TOCNF/BNNS@PDA	5.10(0.58)	1.74	1.33	11.76(1.34)	10	0
	6.24(0.68)	1.79	1.23	13.65(1.49)	20	0
	6.94(0.72)	1.82	1.16	14.59(1.52)	30	0
	9.11(0.74)	1.73	0.95	14.96(1.22)	40	0
	5.77(0.44)	1.45	1.07	8.96(0.68)	60	0
	3.49(0.24)	1.25	1.12	4.89(0.34)	70	0
TOCNF/BNNS@PDA/PL	6.61(0.55)	1.24	1.33	10.85(0.91)	50	4
	4.84(0.37)	1.20	1.28	7.42(0.57)	50	6

	4.48(0.32)	1.18	1.22	6.44(0.46)	50	8

a: h-BN content (50 wt%)

Table S3. The parameters for the calculation of through-plane thermal conductivities of pure TOCNF and different TOCNF-based composite films.

Sample	Thermal Diffusivity (mm^2s^{-1})	Specific heat capacity ($J\ g^{-1}\ K^{-1}$)	Density ($g\ cm^{-3}$)	Thermal conductivity ($W\ m^{-1}\ K^{-1}$)	BNNS @PDA content (wt%)	PL content (wt%)
TOCNF	0.09(0.01)	1.82	0.96	0.16(0.02)	0	0
TOCNF/BN[a]	0.37(0.09)	1.32	1.20	0.58(0.14)	0	0
TOCNF/BNNS @PDA	1.06(0.33)	1.36	1.23	1.76(0.55)	50	0
TOCNF/BNNS @PDA/2%PL	1.16(0.41)	1.29	1.50	2.25(0.79)	50	2

a: h-BN content (50wt%)

Table S4. Comparison of specific through-plane thermal conductivities between

our sample with (50 wt%) BNNS/polymer composites films reported in the paper.

Composites films	Thermal conductivity ($W\ m^{-1}\ K^{-1}$)	Ref.
BNNS/PU	20.65	2
BN/epoxy	6.09	3
f-BNNS/CNF	9.2	4
BNNS/ANF	15.48	5
BNNS/CNF	10.41	6
BNNS/EVA	13.20	7
OH-BNNS/CNF	15.13	8
CNFs/BNNS-p-APP	9.1	9
HPF-BNNSs/PVA	14.5	10
TOCNF/BNNS@PDA/PL	23.49	Our work

PU:polyurethane; CNF: cellulose nanofibers; ANF:aramid nanofiber; EVAl:ethylene-vinyl acetate copolymer; APP: ammonium polyphosphate; PVA:poly(vinyl alcohol)

Table S5. Comparison of specific TCE (TCE per 1 wt% of filler) between our sample with h-BN or BNNS/polymer composites films reported in literatures.

Composites films	TC of composite ($W\ m^{-1}\ K^{-1}$)	Content (wt%)	TCE (%)	Ref.
BNNS/PVA	6.9	94	35.6	11
BNNS/CNF	30.25	70	25.6	4
BNNS/CNF	24.27	60	23.6	12
h-BN/ANF	122.5	70	22.4	13

BNNS/ANF	46.7	30	14.9	14
EP/BNNS	0.999	30	13.23	15
BNNS/epoxy	0.58	20	15.65	16
PGO/BNNS	18.13	25	26.76	17
EP/BNNSs-DOPO-30	1.25	30	16.5	18
TOCNF/BNNS@ PDA/PL	23.49	50	32.5	Our work

EP:epoxy resin; CNF: cellulose nanofibers; ANF:aramid nanofiber; PGO:functionalized GO; DOPO: 6H-dibenz(C,E)(1,2)oxaphosphorin-6-oxide; PVA:poly(vinyl alcohol)

Table S6. TGA data and limiting oxygen index (LOI) of the pure TOCNF and different TOCNF-based composite films.

Sample	T_{onset} (^oC)[a]	T_{max-1} (^oC)[b]	T_{max-2} (^oC)	Char residue (%)	LOI(%)
TOCNF	211.6	245.6	304.1	29.16	18.1
TOCNF/BN	226.8	245.7	305.8	59.14	23.5
TOCNF/BNNS@PDA	223.4	245.2	305.1	64.24	25.7
TOCNF/BNNS@PDA/2% PL	225.5	265.6	319.6	66.18	27.5

TOCNF/BNNS@PDA/4% PL	226.7	265.8	320.3	67.94	29.1
TOCNF/BNNS@PDA/6% PL	227.2	265.9	321.7	70.35	30.5.
TOCNF/BNNS@PDA/8% PL	231.1	267.5	327.2	70.55	31.9

a:T_{onset} refers to the temperature of 5-8 wt% weight loss in the TGA curves.

b:T_{max} is donated as the temperature at maximum weight loss rate.

Table S7. Characteristic parameters of micro-scale combustion calorimetry from the pure TOCNF and different TOCNF-based composite films.

Sample	HRC (J/g·K)	PHRR (W/g)	THR (kJ/g)	TPHRR (°C)
TOCNF	53.1	47.5	7.4	331.1
TOCNF/BN	27.3	20.7	5.9	321.0
TOCNF/BNNS@PDA	42.8	38.1	6.2	327.9
TOCNF/BNNS@PDA/8% PL	17.4	4.8	2.6	347.8

Table S8. Mechanical properties of the pure TOCNF and different TOCNF-based composite films.

Sample	Tensile strength (MPa)	Elongation at break (%)	Young's modulus (GPa)	Work of fracture ($MJ \cdot m^{-3}$)
TOCNF	178.14(8.91)	5.25(0.26)	5.59(0.22)	5.39(0.27)
TOCNF/BN	31.74(1.59)	2.12(0.11)	1.43(0.07)	0.54(0.03)
TOCNF/BNNS@PDA	50.08(2.50)	3.79(0.19)	1.95(0.09)	1.09(0.05)
TOCNF/BNNS@PDA/2%PL	68.30(3.41)	8.93(0.45)	2.13(0.11)	4.20(0.21)
TOCNF/BNNS@PDA/4%PL	32.18(1.61)	3.61(0.18)	2.25(0.11)	0.66(0.03)
TOCNF/BNNS@PDA/6%PL	30.56(1.53)	8.04(0.40)	1.76(0.08)	1.77(0.09)
TOCNF/BNNS@PDA/8%PL	26.85(1.34)	6.13(0.31)	1.48(0.07)	1.18(0.06)
30 wt% BNNS@PDA[a]	84.66(4.23)	6.44(0.32)	3.16(0.16)	3.29(0.16)

a:TOCNF/BNNS@PDA composite film with BNNS@PDA content of 30 wt%.

Table S9. Tensile strength and thermal conductivity comparison of some polymer/BNNS composites.

Composites films	BNNS	Tensile	In-plane Thermal	Ref.

	content (wt%)	strength (MPa)	conductivity (W m^{-1} K^{-1})	
BNNS/cellulose	50	93	4.51	19
BNNS@PDA/ANF	50	36.8	3.94	20
PI/BNNS	50	9.8	0.2	21
BN/PVA	57	17	8.44	22
BNNS/CNF	60	45	24.2	12
HDPE/BNNS	40	25	3.5	23
BNNS/POE	43.75	16	3.6	24
BNNS/PE	50	22	23.03	25
BNNS/GO	50	21.7	10.33	26
TOCNF/BNNS@PDA/PL	50	68.3	23.49	Our work

ANF:aramid nanofiber; PI:polyimide; PVA:poly(vinyl alcohol); CNF: cellulose nanofibers; HDPE:high density polyethylene; POE: polyolefin elastomer; PE: polyethylene; GO:graphene oxide

Reference

1. M. Foygel, R. D. Morris, D. Anez, S. French and V. L. Sobolev, PhRvB, 2005, **71**, 104201.P.-Y. Du, Z.-X. Wang, J.-W. Ren, L.-H. Zhao, S.-L. Jia and L.-C. Jia, *ACS Applied Electronic Materials*, 2022, **4**, 4622-4631.
2. P.-Y. Du, Z.-X. Wang, J.-W. Ren, L.-H. Zhao, S.-L. Jia and L.-C. Jia, *ACS Applied Electronic Materials*, 2022, **4**, 4622-4631.
3. J. Hu, Y. Huang, X. Zeng, Q. Li, L. Ren, R. Sun, J.-B. Xu and C.-P. Wong, *Composites Sci. Technol.*, 2018, **160**, 127-137.
4. K. Wu, J. Fang, J. Ma, R. Huang, S. Chai, F. Chen and Q. Fu, *ACS Appl Mater Interfaces*, 2017, **9**, 30035-30045.
5. L.-H. Zhao, L. Wang, Y.-F. Jin, J.-W. Ren, Z. Wang and L.-C. Jia, *Composites Part B: Engineering*, 2022, **229**.
6. D. Hu, H. Liu, Y. Guo, M. Yang and W. Ma, *Composites Part A: Applied Science and Manufacturing*, 2022, **158**.
7. Z.-G. Wang, W. Liu, Y.-H. Liu, Y. Ren, Y.-P. Li, L. Zhou, J.-Z. Xu, J. Lei and Z.-M. Li, *Composites Part B: Engineering*, 2020, **180**.
8. D. Hu, W. Ma, Z. Zhang, Y. Ding and L. Wu, *ACS Appl Mater Interfaces*, 2020, **12**, 11115-11125.
9. D. Hu, H. Liu, Y. Ding and W. Ma, *Carbohydr. Polym.*, 2021, **264**, 118058.
10. Y. Zhang, H. Wang, T. Xu, L. Wu, H. Niu, X. He, N. Wang and Y. Yao, *J. Appl. Polym. Sci.*, 2022, **139**.
11. X. Zeng, L. Ye, S. Yu, H. Li, R. Sun, J. Xu and C.-P. Wong, Nanoscale, 2015, 7, 6774-6781.
12. K. Wu, P. Liao, R. Du, Q. Zhang, F. Chen and Q. Fu, Journal of Materials Chemistry A, 2018, 6, 11863-11873.
13. G. Xiao, J. Di, H. Li and J. Wang, Composites Sci. Technol., 2020, 189.
14. K. Wu, J. Wang, D. Liu, C. Lei, D. Liu, W. Lei and Q. Fu, Adv. Mater., 2020, 32.
15. G. Han, X. Zhao, Y. Feng, J. Ma, K. Zhou, Y. Shi, C. Liu and X. Xie, Chem. Eng. J., 2021, 407.
16. X. Tian, Y. Li, Z. Chen, Q. Li, L. Hou, J. Wu, Y. Tang and Y. Li, Sci. Rep., 2017, 7.
17. B. Chen, Y. Liu, K. Wu, M. Lu, E. Jiao, J. Shi and M. Lu, J. Therm. Anal. Calorim., 2021, 147, 4047-4058.
18. L. Yang, J. Guo, L. Zhang and C. Li, Ind. Eng. Chem. Res., 2022, 61, 8031-8042.
19. H. Tu, K. Xie, X. Lin, R. Zhang, F. Chen, Q. Fu, B. Duan and L. Zhang, *Journal of Materials Chemistry A*, 2021, **9**, 10304-10315.
20. T. Ma, Y. Zhao, K. Ruan, X. Liu, J. Zhang, Y. Guo, X. Yang, J. Kong and J. Gu, *ACS Appl Mater Interfaces*, 2020, **12**, 1677-1686.
21. J. Wang, D. Liu, Q. Li, C. Chen, Z. Chen, P. Song, J. Hao, Y. Li, S. Fakhrhoseini, M. Naebe, X. Wang and W. Lei, *ACS Nano*, 2019, **13**, 7860-7870.
22. J. Zhang, X. Wang, C. Yu, Q. Li, Z. Li, C. Li, H. Lu, Q. Zhang, J. Zhao, M. Hu

and Y. Yao, *Composites Sci. Technol.*, 2017, **149**, 41-47.
23. X. Zhang, J. Zhang, L. Xia, C. Li, J. Wang, F. Xu, X. Zhang, H. Wu and S. Guo, *ACS Appl Mater Interfaces*, 2017, **9**, 22977-22984.
24. C.-P. Feng, L. Bai, R.-Y. Bao, Z.-Y. Liu, M.-B. Yang, J. Chen and W. Yang, *Advanced Composites and Hybrid Materials*, 2017, **1**, 160-167.
25. C. Yu, J. Zhang, Z. Li, W. Tian, L. Wang, J. Luo, Q. Li, X. Fan and Y. Yao, *Composites Part A: Applied Science and Manufacturing*, 2017, **98**, 25-31.
26. Z. Shen and J. Feng, *ACS Applied Nano Materials*, 2017, **1**, 94-100.